ELSEVIER

MAGMA
Magnetic Resonance Materials in Physics, Biology and Medicine

Magnetic Resonance Materials in Physics, Biology and Medicine 15 (2002) 36–44

www.elsevier.com/locate/magma

# A fast and accurate simulator for the design of birdcage coils in MRI

Giulio Giovannetti [a,*], Luigi Landini [b], Maria Filomena Santarelli [a], Vincenzo Positano [a]

[a] *Institute of Clinical Physiology, National Council of Researches, Via Moruzzi 1, 56124 S. Cataldo, Pisa, Italy*
[b] *Department of Information Engineering, University of Pisa, Pisa, Italy*

Received 22 March 2002; received in revised form 24 May 2002; accepted 5 June 2002

**Abstract**

The birdcage coils are extensively used in MRI systems since they introduce a high signal to noise ratio and a high radiofrequency magnetic field homogeneity that guarantee a large field of view. The present article describes the implementation of a birdcage coil simulator, operating in high-pass and low-pass modes, using magnetostatic analysis of the coil. Respect to other simulators described in literature, our simulator allows to obtain in short time not only the dominant frequency mode, but also the complete resonant frequency spectrum and the relevant magnetic field pattern with high accuracy. Our simulator accounts for all the inductances including the mutual inductances between conductors. Moreover, the inductance calculation includes an accurately birdcage geometry description and the effect of a radiofrequency shield. The knowledge of all the resonance modes introduced by a birdcage coil is twofold useful during birdcage coil design: —higher order modes should be pushed far from the fundamental one, —for particular applications, it is necessary to localize other resonant modes (as the Helmholtz mode) jointly to the dominant mode. The knowledge of the magnetic field pattern allows to a priori verify the field homogeneity created inside the coil, when varying the coil dimension and mainly the number of the coil legs. The coil is analyzed using equivalent circuit method. Finally, the simulator is validated by implementing a low-pass birdcage coil and comparing our data with the literature.


*Keywords:* Birdcage coil; RF magnetic field; Inductances; Software simulator

## 1. Introduction

In 1985 Hayes et al. have firstly described the use of birdcage coils in magnetic resonance imaging systems, by confirming their ability to generate a highly homogenous radio frequency (RF) magnetic field with a high signal to noise ratio (SNR) [1]. We recall that the RF field homogeneity guarantees a uniform atomic nuclei excitation that is a prerequisite to obtain a large field of view (FOV), while the high SNR allows to obtain high quality images. Another important birdcage coil feature is the ability to produce circular polarized field by means of quadrature excitation that increases SNR by a factor of $\sqrt{2}$ [2]. Birdcage coils are widely used in MRI both in low and high field scanners, as transmitter and receiver coils. Birdcage dimensions can vary from about 80 cm diameter and 200 cm length, as in whole-body application, to less than $2 \times 2$ cm as in micro-imaging applications.

The birdcage coils are resonators characterized by more than one resonant mode: in fact, an $N$ legs coil will supply $N/2+1$ distinct resonant modes [3], even if usually the working resonant mode in MRI is the sinusoidal one. On the other hand, the complete spectrum knowledge is required in order to maintain the working mode far away from the other resonant modes to guarantee a perfect tuning of the coil on the precession frequency of the atomic nuclei, according to the Larmor law [4]. Moreover, when the high-pass birdcage coil is employed in open magnet systems [5], another resonant mode, called the Helmholtz mode, apart from the sinusoidal one, is used. In such situation, the frequency localization is useful in order to obtain a quadrature excitation of the birdcage coil. Moreover, the a priori knowledge of the magnetic field pattern is necessary for the birdcage design, since the field homogeneity varies with the coil dimensions and mainly with the legs number [6].

* Corresponding author. Tel.: +39-050-315-2827; fax: +39-050-315-2166
*E-mail address:* giovannetti@ifc.cnr.it (G. Giovannetti).

1352-8661/02/$ - see front matter 
PII: S1352-8661(02)00122-9

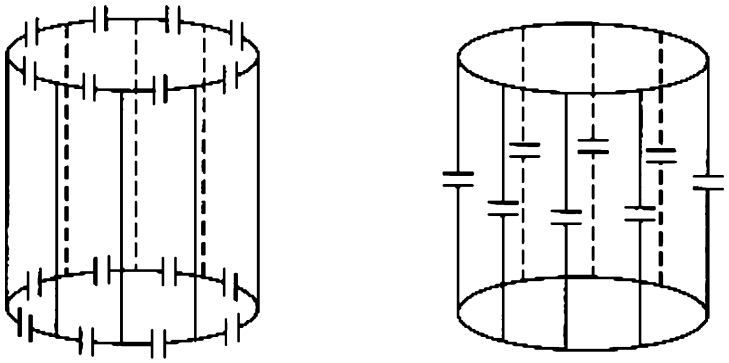

(a) (b)

Fig. 1. (a) High-pass birdcage coil (b) Low-pass birdcage coil.

By means of the birdcage coil equivalent electric circuit [7–9], it is possible to analyze the coil frequency response. In the literature, a number of simulation software have been proposed, as the ones introduced by Jin [10] and Chin [11]: the first one determines the resonance frequency modes carrying out heavy approximations in accounting for mutual inductances, while the second one supplies only the dominant resonance mode instead of the complete frequency spectrum and it does not supply magnetic field patterns. Our simulator allows to obtain, with high accuracy and in short time, not only the dominant frequency mode, but also the complete resonant frequency spectrum and the relevant magnetic field pattern, carefully accounting for the contributions of all the conductors.

It is well known that a shield can be needed in order to minimize interference between birdcage and other coils (i.e. gradient and shim coils) inside the MRI system. The developed software allows to simulate also the shielding contribute, taking into account not only the legs effect [12], but also the coil end-rings.

The accuracy of the developed simulator, based on Interactive Data Language (IDL, Research System) language, derives from the fact that it accounts for all the mutual inductances between coil conductors, wire or strip types. In order to validate the simulator, a low pass birdcage coil prototype has been constructed while an high pass version has been validated using the literature data. Theoretical and measured results confirmed the utility and accuracy of the developed software, also in presence of shielded coil.

## 2. Theory

### 2.1. Birdcage coil circuit analysis

The high-pass and low-pass birdcage coils are characterized by the way in which the capacitors are disposed (Fig. 1). Our method uses an electric equivalent circuit for the birdcage coil simulation based on

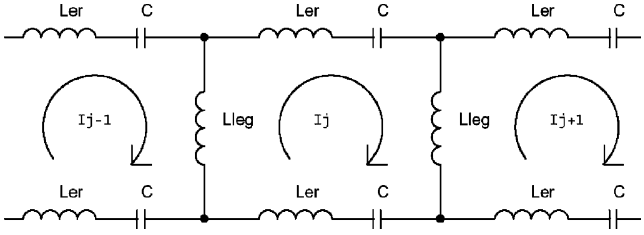


Fig. 2. Segment of the equivalent circuit for a high-pass birdcage coil.

electrical network theory, where conductor is modeled as an inductance. The magnetic field $B_1$ is evaluated by using the Biot–Savart law.

Applying the equivalent electric circuit method, the high pass birdcage coil can be described as the repetition of the electric network segment shown in Fig. 2. In Fig. 2, *Leg* represents the self-inductance of the legs, *C* represents the capacitance of the capacitor between two legs (supposed of the same values) and *Ler* represents the self-inductance of the end-rings segments. We take into account also the mutual inductance: we indicate with $Leg_{j,i}$ (or $Leg_{i,j}$) the mutual inductance between *j*-th and *i*-th legs, with $Ler_{j,i}$ (or $Ler_{i,j}$) the mutual inductance between the conductor that contains the *j*-th capacitor and the conductor that contains the *i*-th capacitor in the same end-ring and with $\bar{L}er_{j,i}$ (or $\bar{L}er_{i,j}$) the mutual inductance between the conductor that contains the *j*-th capacitor and the conductor that contains the *i*-th capacitor in the different end-ring.

By applying the Kirchoff law to the mesh including the *j*-th leg, the $(j+1)$-th leg and the *j*-th capacitor and by considering that $\lambda = 1/\omega^2$, the following matrix equation can be obtained [10,13]:

$$[K]\{I\} = \lambda[H]\{I\} \tag{1}$$

where $\{I\}$ represents a column vector given by: $\{I\} = [I_1, I_2, \ldots, I_N]^T$, $[K]$ and $[H]$ are both $N \times N$ square matrices, whose elements are given by:

$$K_{j,k} = Leg_{j,k} - Leg_{j+1,k} - Leg_{j,k+1} + Leg_{j+1,k+1} + 2(Ler_{j,k} - \bar{L}er_{j,k}) \tag{2}$$

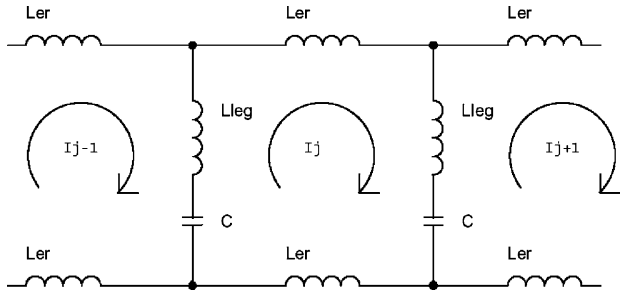


Fig. 3. Segment of the equialent circuit for a low-pass birdcage coil.

$$H_{j,k} = 2\delta_{j,k}/C \tag{3}$$

where $\delta_{j,k}$ is the Kronecker delta, defined as: $\delta_{j,k} = 1$ for $j = k$ and $\delta_{j,k} = 0$ for $j \neq k$.

In order to calculate the solution of Eq. (1) we assume that:

$$\det[K - \lambda H] = 0 \tag{4}$$

Being this determinant a $N$ degree polynomial, Eq. (4) has $N$ solutions ($\lambda_1, \lambda_2, \ldots, \lambda_N$), that correspond to the $N$ resonant frequencies. These $N$ solutions correspond to the eigenvalues in Eq. (1) and for each $\lambda_m$ a solution exists for $\{I\}$ that is indicated as $\{I\}_m$; so, for $N$ solutions of $\lambda$, we obtain $N$ solutions $\{I\}$: $\{I\}_1, \{I\}_2, \ldots, \{I\}_N$ that are the eigenvectors of Eq. (1).

The following considerations arise: (a) the highest resonance frequency corresponds to $m = 0$, that means a constant current in the end-rings and a null current in the legs. To this frequency, the birdcage coil behaves like a Maxwell coil, with equal and opposite currents in the two end-rings. (b) Two contiguous modes (degenerate modes) have the same resonant frequency and generate orthogonal magnetic fields: as we will see later, the first two, corresponding to $m = 1$ and $m = 2$, are able to produce a uniform magnetic field, that is a prerequisite for medical applications with MRI.

It is worth observing that another resonant mode, not accounted in the analysis method herein described, is available in the birdcage coil frequency spectrum. This mode is characterized by equal currents in the same direction in the end-rings, so the birdcage coil behaves as a Helmholtz coil. The relevant resonant frequency is given by [3]:

$$\omega_h = \sqrt{\frac{N}{C\,(L_{ring} + M_{ring})}} \tag{5}$$

where $L_{ring}$ and $M_{ring}$ represent, respectively, the auto inductance of each end-ring and the mutual inductance between them.

The analysis of the birdcage coil in the low-pass version is performed starting from its equivalent circuit, showed in Fig. 3.

In fact, repeating the same identical procedure developed for the high pass version, the matrix equation as in Eq. (1) is obtained, with the only exception that now the matrix $H$ is pentadiagonal in the shape [3]:

$$\begin{array}{ll} H_{j,j-1} = -1/C & H_{i,j} = 2/C \\ H_{j,j+1} = -1/C & H_{1,N} = H_{N,1} = -1/C \\ H_{j,k} = 0 & \text{for others } k \end{array} \tag{6}$$

where $N$ is the number of the legs of the coil.

### 2.2. Shielding

A MRI system uses a set of three coils (gradient coils) for field gradient generation in order to obtain spatial localization information. Compensation coils (shim coils) are also used to increase static magnetic field homogeneity. When a radio frequency field generated by the RF coil is applied, interaction with gradient and shim coils can degrade RF coil performance in terms of signal to noise ratio and they can generate spurious resonant frequencies [10]. In order to avoid such drawback, RF coil is partially shielded. However, the shield strongly modifies resonance frequencies and field distribution in the RF coil. An accurate simulator should include the ability of predicting the resonance frequency shift in dependence of the shield position respect to the birdcage coil.

The shield effect has been studied by means of the images method that assumes that the field produced by induced currents on the shield is identical to the field produced by the original currents images. Because the birdcage coil conductors are parallel to the shield, the image currents have to flow in the opposite direction to the currents in the conductor in order to satisfy the boundary conditions to the shield edges.

As we will see from simulation results, the use of the shield involves the reduction of the auto and mutual inductance values and therefore the resonant frequencies increase. The shield effect can be simulated modifying Eq. (2) by inserting the terms relevant to the mutual inductance between the coils conductors and their images. The approximation that is carried out in order to localize the image currents is that the shield length is much higher than the coil one [10,14]. Because the shield can be locally approximated as a cylindrical surface, the current images that flow in the coil legs can be localized on an imaginary cylinder of radius equal to $R_I = R_S^2/R$ where $R_S$ and $R$ are the shield and birdcage radius, respectively [10,15,16]. It should be stressed that in this study we have seen that partitioning each one of the $N$ segments of the coil end-rings in the sum of a high number of infinitesimal contributes, we can assume that previous approximation is yet valid so we can localize even the images of these conductors in the same virtual cylinder. This technique allows one to predict the RF

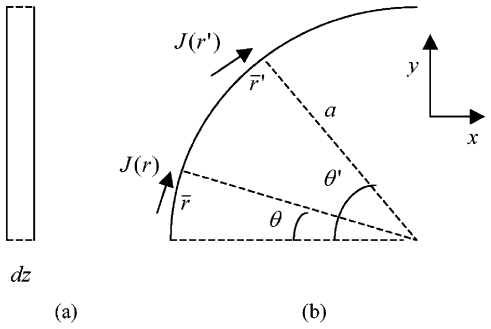


Fig. 4. Segment of end-ring for a strip conductor.

shield effect in a more accurate manner with respect to other simulators.

## 3. Materials and methods

### 3.1. Analytical simulation of inductances and magnetic fields

As far as the analysis and the design of radio frequency coils, it is necessary to evaluate the conductor self-inductance and the mutual inductance between the two conductors. The self-inductance of a conductor, which is fed with a current density $J$ is evaluated by means of the following expression [10]:

$$L = \frac{\mu_0}{4\pi I^2} \iiint_V \iiint_V \frac{J(r) \cdot J(r')}{R} \, dv \, dv' \tag{7}$$

where $\mu_0$ is the permeability of free space, $I$ represents the total current in the conductor, $V$ is the conductor volume and $R = | r - r' |$.

By assuming that the current is uniformly distributed over the surface of the strip, the evaluation of the self-inductance of a strip of width $w$, length $l$ and negligible thickness can be approximated by a very simple formula [17]:

$$L = \frac{\mu_0 l}{2\pi}\left(\ln\frac{2l}{w} + \frac{1}{2}\right) \tag{8}$$

whose accuracy increases as $l$ is large with respect to $w$.

This formula can be used to calculate the self-inductance of the birdcage coil legs (*Lleg*), because the strip width is much lower than the coil length. In order to accurately take into account the end-ring shape (with respect to the approximations made by the other simulators or by the literature data, see [18]), we consider the conductor segments that constitute the birdcage end-rings, as outlined in Fig. 4: (a) lateral and (b) upper side birdcage views.

Referring to Eq. (7), the infinitesimal surfaces are given by the following expressions:

$$\begin{aligned} ds &= a \, d\theta \, dz \\ ds' &= a \, d\theta' \, dz' \end{aligned} \tag{9}$$

while the points coordinates $\bar{r}$ and $\bar{r}'$ are given by:

$$\begin{aligned} \bar{r} &\equiv (x,\ y,\ z) \equiv (a\cos\theta,\ a\sin\theta,\ z) \\ \bar{r}' &\equiv (x',\ y',\ z') \equiv (a\cos\theta',\ a\sin\theta',\ z') \end{aligned} \tag{10}$$

The term in Eq. (7) given by the scalar product of the current densities divided by the square of the total current becomes:

$$\frac{J(r) \cdot J(r')}{I^2} = \frac{1}{w^2}\cos(\theta' - \theta) \tag{11}$$

where $w$ is the conductor strip width. The distance $R$ between the two points is given by:

$$\begin{aligned} R &= \sqrt{(x-x')^2 + (y-y')^2 + (z-z')^2} \\ &= \sqrt{[a\cos\theta - a\cos\theta']^2 + [a\sin\theta - a\sin\theta']^2 + (z-z')^2} \end{aligned} \tag{12}$$

The final expression that allows to calculate the self-inductance value of an end-ring segment, is constituted by a quadruple integral, in which $dz$ and $dz'$ are integrated from 0 to $w$ (strip width of the conductor), while $d\theta$ and $d\theta'$ are integrated from 0 to $2\pi/N$ (length of the segment over the ring, being $N$ the number of the birdcage legs):

$$L = \frac{\mu_0}{4\pi w^2} \int_{-w/2}^{w/2} \int_0^{2\pi/N} \int_{-w/2}^{w/2} \int_0^{2\pi/N} \frac{\cos(\theta'\text{-}\theta)a^2}{R} \, dz \, dz' \, d\theta \, d\theta' \tag{13}$$

As far as the mutual inductance calculation, we consider two conductors with current density $J_1$ and $J_2$ across $V_1$ and $V_2$ volumes. Assuming that $I_1$ and $I_2$ are the total currents in the $V_1$ and $V_2$ volumes respectively, the mutual inductance expression between the two conductors is given by [10]:

$$\begin{aligned} M_{12} &= M_{21} \\ &= \frac{\mu_0}{4\pi I_1 I_2} \iiint_{V1} \iiint_{V2} \frac{J_1(r) \cdot J_2(r')}{R} \, dv \, dv' \end{aligned} \tag{14}$$

If the strip width is much lower than the distance $d$ between two parallel conductors of the same length $l$ (as the legs of the birdcage coil), the solution of Eq. (14) can be approximated by the following equation [17]:

$$\begin{aligned} M_{12} &= M_{21} \\ &= \frac{\mu_0 l}{2\pi}\left[\ln\left(\frac{l}{d} + \sqrt{1 + \frac{l^2}{d^2}}\right) - \sqrt{1 + \frac{d^2}{l^2}} + \frac{d}{l}\right] \end{aligned} \tag{15}$$

As far as the mutual inductance evaluation between the segments that constitute the coil end-rings, the relevant formula is the one that allows to calculate the ring segment self-inductance (Eq. (13)). The only difference is that in the case of the mutual inductance

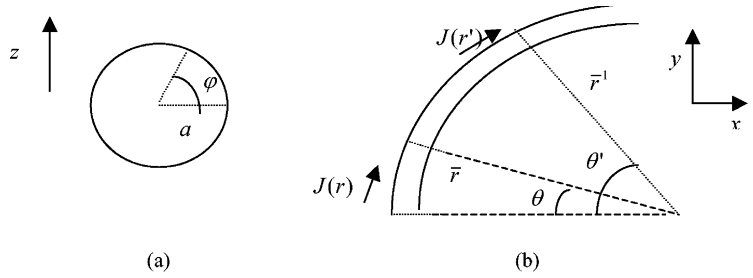


Fig. 5. Segment of end-ring for a wire conductor.

the integration extremes are referred to two distinct segments, that is:

$$M=\frac{\mu_0}{4\pi w^2}\int_{-w/2}^{w/2}\int_{j2\pi/N}^{(j+1)2\pi/N}\int_{-w/2}^{w/2}\int_{k2\pi/N}^{(k+1)2\pi/N}\times\frac{\cos(\theta'-\theta)a^2}{R}\,\mathrm{d}z\,\mathrm{d}z'\,\mathrm{d}\theta\,\mathrm{d}\theta' \tag{16}$$

where $j$ and $k$ characterize two ring segments.

In the case of cylindrical symmetrical conductors (wire), by assuming that the current is uniformly distributed over the surface of the wire, the Eq. (7) is used for the self-inductance calculation of a wire of radius $a$ and length $l$ that can be approximated by the following formula [17]:

$$L=\frac{\mu_0 l}{2\pi}\left(\ln\frac{2l}{a}-1\right) \tag{17}$$

whose accuracy increases as $l$ increases with respect to $a$. This is the formula used for the self-inductance calculation of the birdcage coil legs (*Lleg*) made by cylindrical wire.

Let us consider the conductor segments that constitute the birdcage end-rings, as drawn in Fig. 5: (a) section (b), upper view ($R$ indicates the birdcage radius at the end-rings center distance and $a$ the cylindrical wire radius).

Remembering Eq. (7), the surface infinitesimal calculated in spherical coordinates, are given by the following expressions:

$$\begin{aligned}\mathrm{d}s&=a(R+a\cos\varphi)\,\mathrm{d}\varphi\,\mathrm{d}\theta\\ \mathrm{d}s'&=a(R+a\cos\varphi')\,\mathrm{d}\varphi'\,\mathrm{d}\theta'\end{aligned} \tag{18}$$

while the points $\bar{r}$ and $\bar{r}'$ coordinates are given by:

$$\begin{aligned}\bar{r}&\equiv(x,\ y,\ z)\\ &\equiv(R\cos\theta+a\cos\varphi\cos\theta,\ R\sin\theta\\ &\quad+a\cos\varphi\sin\theta,\ a\sin\varphi)\\ \bar{r}'&\equiv(x',\ y',\ z')\\ &\equiv(R\cos\theta'+a\cos\varphi'\cos\theta',\ R\sin\theta'\\ &\quad+a\cos\varphi'\sin\theta',\ a\sin\varphi')\end{aligned} \tag{19}$$

The term given by the scalar product of the current density divided by the square of the total current becomes:

$$\frac{J(r)\cdot J(r')}{I^2}=\frac{1}{(2\pi a)^2}\cos(\theta'-\theta) \tag{20}$$

where $a$ is the conductor radius.

The distance $R$ between the two points is given by:

$$R=\sqrt{(x-x')^2+(y-y')^2+(z-z')^2} \tag{21}$$

The final expression that allows to calculate the self-inductance value of a cylindrical conductor segment that constitutes the end-rings, is made of a quadruple integral, in which $\mathrm{d}\varphi$ and $\mathrm{d}\varphi'$ are integrated from 0 to $2\pi$ (on the section of the conductor that constitutes the segment), while $\mathrm{d}\theta$ and $\mathrm{d}\theta'$ are integrated from 0 to $2\pi/N$ (length of the segment over the ring, being $N$ the number of birdcage coil legs):

$$L=\frac{\mu_0}{4\pi(2\pi a)^2}\int_0^{2\pi2\pi/N}\int_0^{2\pi2\pi/N}\int_0^{2\pi2\pi/N}\int_0^{2\pi2\pi/N}\frac{\cos(\theta'-\theta)}{R}\,a^2(R+a\cos\varphi)\times(R+a\cos\varphi')\,\mathrm{d}\varphi'\,\mathrm{d}\theta'\,\mathrm{d}\varphi\,\mathrm{d}\theta \tag{22}$$

Since the conductor dimension is small with respect to the distance among legs, the evaluation of the mutual inductance evaluation along the birdcage coil legs is carried out using Eq. (15). Moreover, the mutual inductance evaluation between different end-ring segments uses Eq. (22), already applied to calculate the ring segment self-inductance, by changing the mutual inductance integration extremes as follows:

$$M=\frac{\mu_0}{4\pi(2\pi a)^2}\int_0^{2\pi(j+1)2\pi/N}\int_{j2\pi/N}^{2\pi(k+1)2\pi/N}\int_0^{2\pi2\pi/N}\int_{k2\pi/N}^{2\pi2\pi/N}\times\frac{\cos(\theta'-\theta)}{R}\,a^2(R+a\cos\varphi)\times(R+a\cos\varphi')\,\mathrm{d}\varphi'\,\mathrm{d}\theta'\mathrm{d}\varphi\,\mathrm{d}\theta \tag{23}$$

where $j$ and $k$ individualize two ring segments.

The case of the wire conductors coil can be studied using the strip conductors formula as follows: Eqs. (8) and (17) are made equal and conductors are assumed to

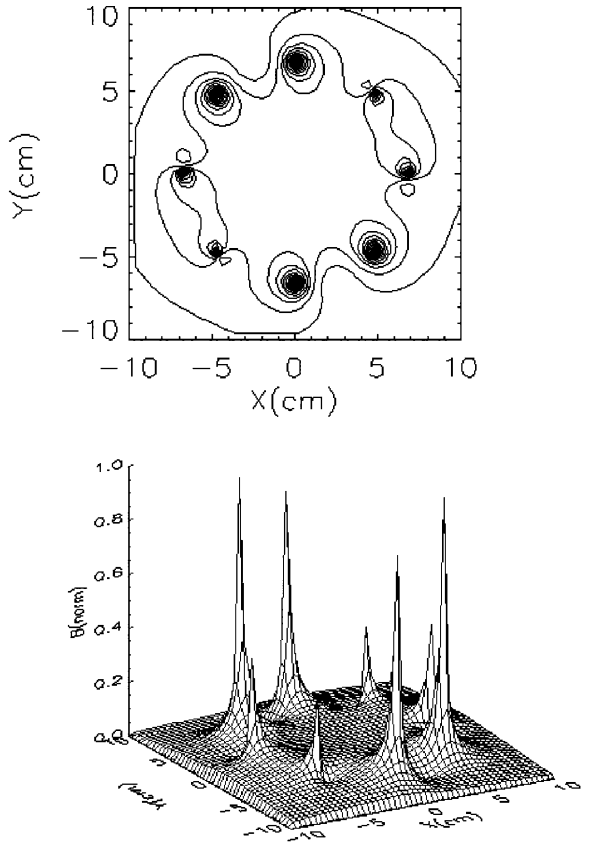


Fig. 6. Contour and 3D plots of the $B_1$ field of an 8 legs low-pass birdcage coil for mode 1.

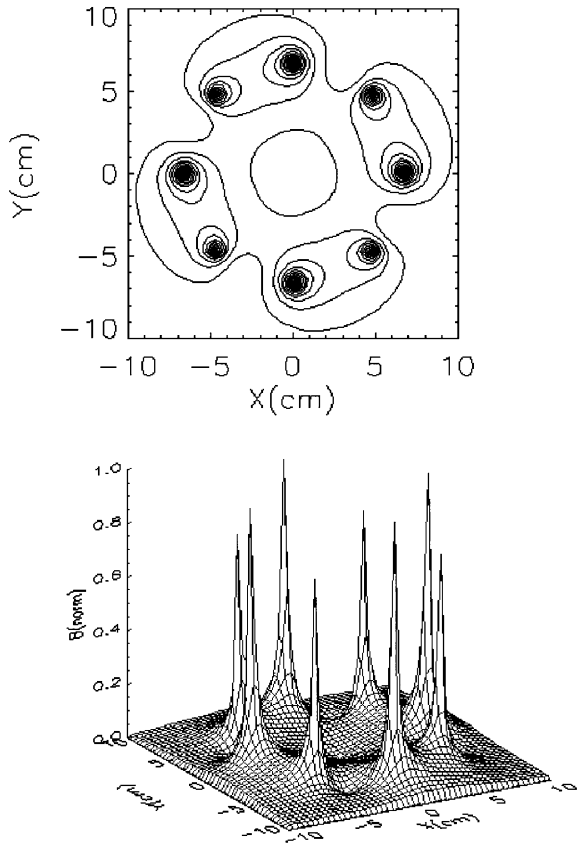


Fig. 7. Contour and 3D plots of the $B_1$ field of an 8 legs low-pass birdcage coil for mode 3.

have the same length $l$. Carrying out simple mathematical operations, a relationship is obtained that allows to evaluate the equivalent width $w$ of a wire of radius $a$[10]:

$$w = 4.482\, a \tag{24}$$

In order to perform magnetic field analysis for a birdcage coil, the Biot-Savart equation is used. The use of this theory that implies a nearly static magnetic field assumption is valid when the coil dimensions are much lower than the wavelength. This assumption is often verified at frequencies routinely used in MRI applications, so that the simulator can be effectively used for the MR birdcage coils design. As an example, at 1.5 T the related wavelength is 4.7 m and the nearly static assumption holds for any birdcage dimensions. Increasing the magnetic field strength, the approximation holds as the coil dimension decreases. For instance, at 6 T (255 MHz frequency, 1.7 m wavelength) the Biot–Savart equation can yet used for small birdcage coils. In order to calculate the magnetic field generated by the currents along the birdcage conductors, the coil can be subdivided in legs and in end-ring segments in order to separately study their total field contribution.

For this purpose, the birdcage conductors strip width (or the wire radius) can be neglected with respect to the wavelength in order to treat them as very thin wires.

## 4. Results and discussions

The software used for the birdcage coil simulator was developed using the IDL 5.4 (Interactive Data Language) environment, distributed by the Research Systems. The program is able to evaluate all the coil resonant frequencies and to plot magnetic field distribution diagrams as contours (level curves), 3D representation and axial sections. The time required for a typical analysis (i.e. 8 legs birdcage) is about 30 s on 1 GHz Pentium based PC. The source code is available on request.

The input parameters are the coil dimensions (length, radius and legs number), the conductor dimensions (strip width or wire radius), the capacitor value and the $z$ coordinate to which the field diagram refers.

The diagrams herein discussed are relevant to a coil whose inferior end-ring lies on the $x$, $y$ plane and centered at $x = 0$ and $y = 0$.

The diagrams in Figs. 6–9 refer to magnetic field patterns relevant to a low-pass birdcage coil with $N = 8$ legs, length 11 cm, diameter 13.4 cm, conductors constituted by 1 cm width strips and referred to a $z$ coordinate equal to half the coil length.

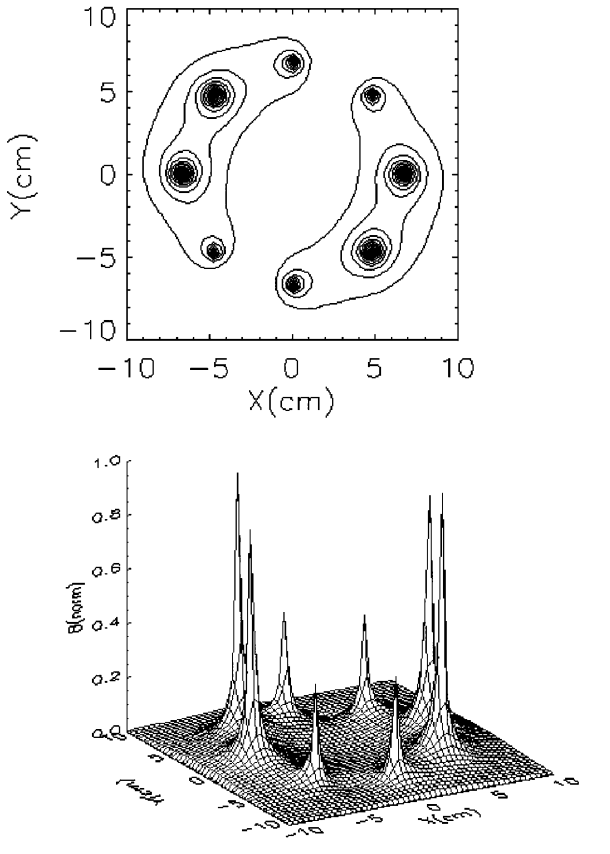


Fig. 8. Contour and 3D plots of the $B_1$ field of an 8 legs low-pass birdcage coil for mode 5.

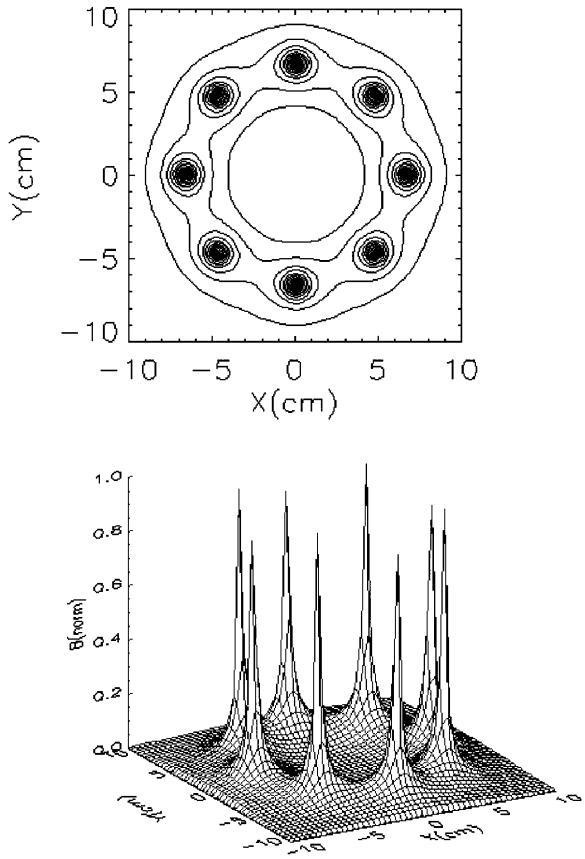


Fig. 9. Contour and 3D plots of the $B_1$ field of an 8 legs low-pass birdcage coil for mode 7.

The low-pass version of the birdcage simulation corresponds to a highly uniform modes 1 and 2 (sinusoidal modes) magnetic field (Fig. 6 shows the magnetic field for the mode 1).

In order to verify the magnetic field homogeneity produced inside the coil, we refer to Fig. 10, obtained carrying out an axial section of the birdcage coil and plotting the mode 1 field.

In order to validate the simulator, a birdcage coil has been realized using a 12 cm in height and 13.4 cm in diameter plexiglass cylinder; on such cylinder a 1 cm width and 35 μm thickness adhesive strip was applied in order to obtain a 11 cm in length birdcage coil. The contact points among the different legs and the end-rings segments were melted in order to obtain electric continuity.

Along the legs, 2 nF capacities were introduced using two 1 nF capacitors (ATC 100B-American Technical Ceramics, USA) with a high quality factor ($Q > 10\,000$ at 1 MHz). Fig. 11 shows the prototype coil.

The coil has been tested using a network analyzer (HP 3577 A) and a dual-loop probe [19]. In Table 1 the comparison between theoretical and measured resonant frequencies is reported, showing a deviation lower than 2.2%. Such deviation is compatible with the capacitors tolerances used in the birdcage coil construction.

For the same coil, the resonant frequency of the dominant mode obtained using the two simulators available in the literature is 9.291 MHz [10] and 7.730 MHz [11], with an accuracy of 15 and 4.3%, respectively (see Table 1).

To experimentally verify the magnetic field pattern generated by the simulator, we measured the field uniformity for the sine wave mode in the central transverse planes perpendicular to the birdcage coil axis, obtaining a satisfactory value of 72%.

The simulator was also tested when the coil is shielded. Two cylinders were built and shielded with conductor material, of 16 and 24 cm diameters, respectively. In Tables 2 and 3 the theoretical and measured resonant frequencies show a good agreement (the error is below 4.2 and 1.6%, respectively, while the simulator in [10] provides frequencies with an error of 9.3 and 11.6%, respectively), demonstrating the accuracy of our approach to simulate the RF shielding contribute.

We have also tested the simulator using data described in the literature [20] for a high-pass birdcage coil tuned at a much greater frequency than the low-pass prototype herein developed; the comparisons are shown in Table 4, giving evidence of a deviation lower than 4.5% (while the other simulator gives an error of 8.8%).

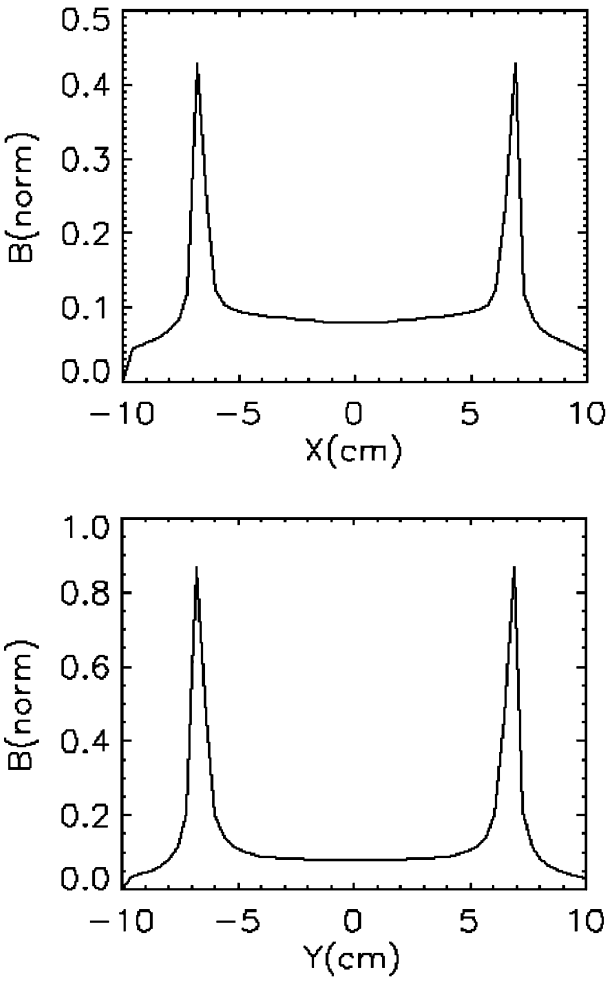


Fig. 10. Axial sections plots ($x$ = constant and $y$ = constant) of the simulated $B_1$ field of an 8 legs low-pass birdcage coil for mode 1.

Fig. 11. Illustration of the built low-pass birdcage coil.

Table 1
Comparison between predicted and measured resonant frequencies (MHz) of the built LP birdcage coil with our simulator, simulator 1 [10] and simulator 2 [11]

| Mode | Our simulator | Measured | Simulator 1 | Simulator 2 |
|---|---|---|---|---|
| 1 | 8.259 | 8.081 | 9.290 | 7.730 |
| 3 | 12.044 | 12.075 | 12.383 | – |
| 5 | 13.695 | 13.875 | 13.718 | – |
| 7 | 14.174 | 14.475 | 14.113 | – |

Table 2
Comparison between predicted and measured resonant frequencies (MHz) of a shielded LP birdcage coil (radius of the shield: 8 cm) with our simulator and simulator 1 [10]

| Mode | Our simulator | Measured | Simulator 1 |
|---|---|---|---|
| 1 | 10.423 | 10.004 | 10.938 |
| 3 | 13.918 | 13.887 | 14.067 |
| 5 | 15.105 | 15.252 | 15.086 |
| 7 | 15.416 | 15.707 | 15.353 |

Table 3
Comparison between predicted and measured resonant frequencies (MHz) of a shielded LP birdcage coil (radius of the shield: 12 cm) with our simulator and simulator 1 [10]

| Mode | Our simulator | Measured | Simulator 1 |
|---|---|---|---|
| 1 | 8.543 | 8.412 | 9.390 |
| 3 | 12.185 | 12.237 | 12.417 |
| 5 | 13.744 | 13.962 | 13.695 |
| 7 | 14.199 | 14.450 | 14.075 |

Table 4
Comparison between predicted and measured resonant frequencies (MHz, see Ref. [20]) of a HP birdcage coil with our simulator and simulator 1 [10]

| Mode | Our simulator | Measured | Simulator 1 |
|---|---|---|---|
| 1 | 78.055 | 74.650 | 81.222 |
| 3 | 56.376 | 57.450 | 56.472 |
| 5 | 47.750 | 48.880 | 47.464 |
| 7 | 45.350 | 46.780 | 45.009 |

It proves the simulator is highly efficient also for frequencies routinely used in MRI applications.

## 5. Conclusions

The present article describes the implementation of a birdcage coil simulator, in the high-pass and low-pass versions in order to supply, with high accuracy, all the

coil resonant modes, also when the coil is shielded. Moreover, the developed software allows a priori knowledge of the magnetic field pattern inside the coil, thus verifying the homogeneity degree.

The first innovation of this simulator respect to the others described in literature is the ability to simulate more accurately the effect of the RF shield, including the effect of the end-ring segments. Moreover the software takes into account the mutual inductances between all the conductors. Finally, the end-ring segments inductance calculation is done by accounting for the segment geometry. The simulator has been validated for a low-pass birdcage coil by measuring the resonant frequency modes in a real birdcage home-built for this purpose, and for a high-pass version by using data available in the literature. The test allowed one to evaluate the accuracy degree of the developed simulator. The proposed simulator was demonstrated to be able to obtain a complete resonant frequency spectrum and the relevant magnetic field pattern with high accuracy and in short time.

## Acknowledgements

The authors thank Professor J. Jin (University of Illinois, Urbana), Professor P.M. Joseph (Hospital of University of Pennsylvania, Philadelphia), Professor D.I. Hoult (National Research Council Canada) and Dr C.L. Chin (University of Pennsylvania, Philadelphia) for providing helpful comments and encouragement. Particular thanks to R. Francesconi (Institute of Clinical Physiology, C.N.R., Pisa) for his useful help in the building of the coil.

## References

[1] Hayes CE, Edelstein WA, Schenck JF, Mueller OM, Eash M. An efficient, highly homogeneous radiofrequency coil for whole-body NMR imaging at 1.5 T. J Magn Reson 1985;63:622–8.
[2] Chen CN, Hoult DI, Sank VJ. A further $\sqrt{2}$ improvement in sensitivity. J Magn Reson 1983;54:324–7.
[3] Leifer MC. Resonance modes of the birdcage coil. J Magn Reson 1997;124:51–60.
[4] Khandpur RS. Handbook of Biomedical Instrumentation. New York: MacGraw-Hill, 1991.
[5] Fujita H, Braum WO, Morich MA. Novel quadrature birdcage coil for a vertical $B_0$ field open MRI system. Magn Reson Med 2000;44:633–40.
[6] Crozier S, Luescher K, Forbes LK, Doddrell DM. Optimized small-bore, high-pass resonator designs. J Magn Reson 1995;109(Series B):1–11.
[7] Tropp J. The theory of the bird-cage resonator. J Magn Reson 1989;82:51–62.
[8] Pascone R, Vullo T, Farrelly J, Cahill PT. Explicit treatment of mutual inductance in eight-column birdcage resonators. Magn Reson Imag 1992;10:401–10.
[9] Tropp J. Mutual inductance in the bird-cage resonator. J Magn Reson 1997;126:9–17.
[10] Jin J. Electromagnetic Analysis and Design in Magnetic Resonance Imaging. Boca Raton, FL: CRC Press, 1999.
[11] Chin CL, Dardzinski BJ, Li S, Smith MB. Software development for accurate and efficient birdcage coil design. ISMRM 6th Scientific Meeting, Sydney, Australia, April 18–24, 1998, p. 653.
[12] Joseph PM, Lu D. A technique for double resonant operation of birdcage imaging coils. IEEE Trans Med Imag 1989;8:286–94.
[13] Shen GX, Wu JF, Boada FE, Thulborn KR. Experimental verified, theoretical design of dual- tuned, low-pass birdcage radiofrequency resonators for Magnetic Resonance Imaging and Magnetic Resonance Spectroscopy of human brain at 3.0 Tesla. Magn Reson Med 1999;41:268–75.
[14] Jin J, Magin RL, Shen G, Perkins T. A simple method to incorporate the effects of an RF shield into RF resonator analysis for MRI applications. IEEE Trans Biomed Eng 1995;42:840–3.
[15] Li S, Collins CM, Dardzinski BJ, Chin CL, Smith MB. A method to create an optimum current distribution and homogeneous $B_1$ field for elliptical birdcage coils. Magn Reson Med 1997;37:600–8.
[16] Collins CM, Li S, Yang QX, Smith MB. A method for accurate calculation of $B_1$ fields in three dimensions. Effects of shield geometry on field strength and homogeneity in the birdcage coil. J Magn Reson 1997;125:233–41.
[17] Grover FW. Inductance Calculations: Working Formulas and Tables. New York: Dover, 1962.
[18] Chin C, Li S, Collins CM, Smith MB. Mutual inductance calculations between end-ring segments for elliptical birdcage coils. ISMRM 5th Scientific Meeting, Vancouver, BC, Canada, April 12–18, 1997, p. 1498.
[19] Darrasse L, Kassab G. Quick measurement of NMR-coil sensitivity with a dual-loop probe. Rev Sci Instrum 1993;64:1841–4.
[20] Pascone RJ, Garcia BJ, Fitzgerald TM, Vullo T, Zipagan R, Cahill PT. Generalized electrical analysis of low-pass and high-pass resonators. Magn Reson Imag 1991;9:395–408.